RESEARCH PAPER

Effect of beam deviation on electron beam welded Ti-22Al-25Nb/TC4 dissimilar alloys

Shaogang Wang[1] · Yuan Chen[1] · Lize Li[1]

Abstract

Dissimilar alloys of Ti-22Al-25Nb (at%) and TC4 are welded by electron beam welding (EBW), and the effect of different welding procedures (with electron beam deviation to TC4 side or without) on microstructure and mechanical properties of welded joints are investigated. Results show that the microstructure of fusion zone (FZ) consists of B2 phase and martensitic α' phase. The heat-affected zone (HAZ) of Ti-22Al-25Nb side near FZ consists of B2 phase and a little of α_2 phase, and that of TC4 side near FZ is the α' phase. When the electron beam is deviated to TC4 side 0.15 mm during welding, the welded joint with good appearance of weld can be obtained, and the ultimate tensile strength and elongation of welded joint reach 967.6 MPa and 3.1%, respectively. The variation of microhardness in weld zone with beam deviation is smaller that of without beam deviation. Electron beam oscillation can stir fully the molten pool during welding, and the main alloying elements distribute uniformly in FZ. On the whole, the mechanical performance of welded joint with beam deviation is better than that of without beam deviation.

Keywords Ti$_2$AlNb alloy · Dissimilar alloys · Electron beam welding · Beam deviation · Microstructure · Mechanical property

1 Introduction

In recent years, TiAl alloys such as Ti$_2$AlNb alloy were paid more attention and much effort had been done on their application in engine parts, for example the compressor whose operating temperature is at the range of 600–700 °C [1, 2]. Compared with that of Ni-based superalloys, TiAl alloys have a higher strength-to-weight ratio at high temperature, and they have good ability to anti-oxidation and corrosion resistance under the ambient atmosphere and high alternating load [3]. However, there are disadvantages of TiAl alloys, such as high brittleness at room temperature, difficult processing (poor weldability), and high cost. On the other hand, the $\alpha + \beta$ type titanium alloy TC4 (Ti-6Al-4V) has been widely used in aerospace field, such as aircraft structures and engine parts, due to its excellent fracture toughness, high specific strength, long

✉ Shaogang Wang
  sgwang@nuaa.edu.cn

[1] College of Material Science and Technology, Nanjing University of Aeronautics and Astronautics, Nanjing 211106, China

fatigue life, and good corrosion resistance [4, 5]. At present, TC4 alloy is the primary structural material applied to engine parts at the temperature range of 500–600 °C [4].

In industrial fields, under the premise of meeting the service requirements, the application of dissimilar metal components is convenient and low cost. Welding processes are widely used to fabricate dissimilar metal components. Casalino and Mortello [6] investigated the fiber laser offset welding of Al-Ti (AA5754-Ti6Al4V) butt joints. Due to its excellent mechanical performance at high temperature, as one of the improved TiAl alloys, Ti$_2$AlNb alloy is regarded as a potential structural material instead of Ni-based superalloys and TC4 alloy in aerospace applications. However, some structural components made by single Ti$_2$AlNb alloy are not reasonable from the viewpoint of manufacturing process and product cost. As described above, Ti$_2$AlNb and TC4 alloys can be applied to the engine parts at different operating temperatures. Consequently, it is of great significance to join TC4 and Ti$_2$AlNb alloys for the potential application in the future.

Recent studies on the joining of Ti alloy and Ti$_2$AlNb alloy were mainly focused on high energy density beam welding, such as laser beam welding (LBW) and electron beam welding (EBW). Zhang et al. [7] investigated the microstructure and tensile properties of Ti-22Al-27Nb/TA15 dissimilar joints by LBW. Shen et al. [8, 9] used single-beam and dual-beam laser to weld

Table 1 Electron beam welding parameters of dissimilar metals

Sample no.	Welding process	Electron beam current (mA)	Focusing current (mA)	Heat input (J/mm)	Deviation distance to TC4 side (mm)
#1	First bead welding	14.5	413	65.25	0
	Modification welding	11.5	387	51.75	
#2	First bead welding	14.5	413	65.25	0.15
	Modification welding	11.5	387	51.75	
#3	First bead welding	13.0	413	58.50	0
	Modification welding	10.0	387	45.00	
#4	First bead welding	13.0	413	58.50	0.15
	Modification welding	10.0	387	45.00	
#5	First bead welding	12.5	413	56.25	0
	Modification welding	9.5	387	42.75	
#6	First bead welding	12.5	413	56.25	0.15
	Modification welding	9.5	387	42.75	

Ti-22Al-25Nb/TA15 dissimilar alloys respectively. Lei et al. [10] investigated the microstructural evolution of Ti-22Al-27Nb/TC4 dissimilar joint by LBW. Results showed that the FZ consisted of martensitic α' and B2 phases. The heat-affected zone (HAZ) of Ti-22Al-27Nb side was composed of B2 and coarse α_2 phases, and the HAZ of TC4 side was made up of primary α, acicular α, and martensitic α' phases.

Compared with LBW, EBW has the advantages to join dissimilar metals between Ti alloy and Ti$_2$AlNb alloy, due to its vacuum environment and high welding efficiency. Some investigations had been conducted on the dissimilar joints of Ti$_2$AlNb and TC11 alloys by EBW. Tan et al. [1, 11] studied the effect of post-weld heat treatment (PWHT) and isothermal deformation on microstructure and mechanical properties of joints between Ti$_2$AlNb and TC11 alloys by EBW. Qin et al. [12] joined dissimilar alloys Ti-24Al-15Nb-1.5Mo, and TC11 by EBW, and the effect of hot working on stress rupture properties of joint was investigated. Up to now, there are few reports on the joining of dissimilar alloys Ti-22Al-25Nb and TC4 by EBW. Generally, the microstructure and mechanical properties of joints are greatly influenced by different welding parameters, the original microstructure and chemical compositions of base metals. In present work, dissimilar alloys TC4 and Ti-22Al-25Nb are welded by EBW, and the microstructural evolution and mechanical properties of the welded joints are systematically investigated.

2 Materials and experimental procedure

The base metals are Ti-22Al-25Nb (at%) and TC4 (Ti-6Al-4 V) with the thickness of 3.5 mm. The welding samples are prepared to the dimension of 60 mm × 50 mm × 3.5 mm, and the butt joint is used. Before welding, the welding samples are polished by sand paper, and then cleaned with solution (10 mL HF + 30 mL HNO$_3$ + 60 mL H$_2$O), and rinsed with water and dried. The ZD60-6A type electron beam welding machine is

used to join the two dissimilar metals along the longitudinal direction of samples. The electron beam welding machine is designed and made by oneself, and it has the maximum accelerating voltage of 60 kV.

Chen at al. [13] reported that when the electron beam was deviated towards TC4 alloy side during welding, the low content of element Al in weldment could improve the mechanical properties of welded joint. In present work, electron beam aims at the weld center or is deviated to TC4 alloy side with the distance of 0.15 mm respectively. The molten pool could be stirred fully by electron beam oscillation, thus gases easily escaped from weldment and the distribution of alloying elements became uniform in FZ [14]. As a result, the mechanical properties of joints can be greatly improved. Electron beam oscillation with the circular pattern is carried out, and the oscillation frequency is 500 Hz. In order to improve the appearance of weld, the modification welding is conducted after the first bead welding. During welding, the proper welding condition needs to be selected. After some attempt welding, the optimized welding parameters are determined based on the appearance of weld and the stability of welding process. Namely, the pressure of vacuum chamber is 5×10^{-4} Pa, accelerating voltage 50 kV, welding speed 10 mm/s, and working distance 300 mm. The other welding parameters are listed in Table 1. Weld heat input is calculated by the following equation.
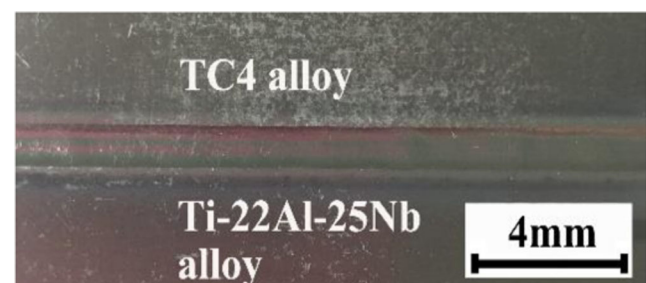

Fig. 1 Appearance of weld

$$E = \eta UI/v \qquad (1)$$

where E is the heat input, U is the accelerating voltage, I is the electron beam current, η is the welding efficiency of EBW and its value is taken as 90% [15], and v is the welding speed.

After welding, the microstructure of welded joints is observed by using a MR-500 optical microscope (OM) and a JSM-6360LV scanning electron microscope (SEM) respectively. D8 Advance X-ray diffractometer (XRD) is used to identify the phase constituent of weldment. Energy dispersive spectrometer (EDS) is used to inspect the distribution of alloying elements in weld zone. According to the standard GB/T 2651-2008/ISO 4136:2001, tensile tests are performed at room temperature by using CMT-5105 universal electronic material machine with the displacement speed of 1 mm/min. The tensile fracture mode of welded joint is investigated by using SEM. HXS-1000A hardness tester is used to measure the microhardness of weld zone, and the test condition is that with the load of 200 g and duration time of 15 s.

3 Results and discussion

3.1 Morphology of weld

The macrograph of joint #2 is shown in Fig. 1. The appearance of weld is good, and no welding defect is found on the surface of welded joint, which demonstrates that the welding procedure is feasible. The cross section of weldment presents nail-shape, as shown in Fig. 2. The fusion boundary at the Ti-22Al-25Nb interface is smooth and linear, while the fusion boundary at the TC4 interface is discontinuous and curved. Cross section of the welded joint can be further divided into five zones, namely FZ, near-HAZ, far-HAZ, and two base metal zones. The FZ is composed of two parts: the first bead welding zone which presents the deep penetration characteristic of EBW and the modification welding zone formed by the subsequent modification welding. No welding defects such as crack or porosity are generated in weld metal. However, owing to the relatively low electron beam current and beam deviation to TC4 side during welding, it has not enough energy to cause suck back in the joint #6, as shown in Fig. 3.

Because the physical properties involving melting point, thermal expansion coefficient, thermal expansion coefficient and thermal conductivity between Ti-22Al-25Nb and TC4 alloys were different [16, 17], there was an obvious difference in molten area between the two base metals during welding. According to the welding procedures of electron beam deviation to assembly center or not, the molten zones of Ti-22Al-25Nb and TC4 alloy sides are determined respectively, as shown in Fig. 4. When the electron beam is deviated to TC4 side with a distance of 0.15 mm, as shown in Fig. 4 a, the
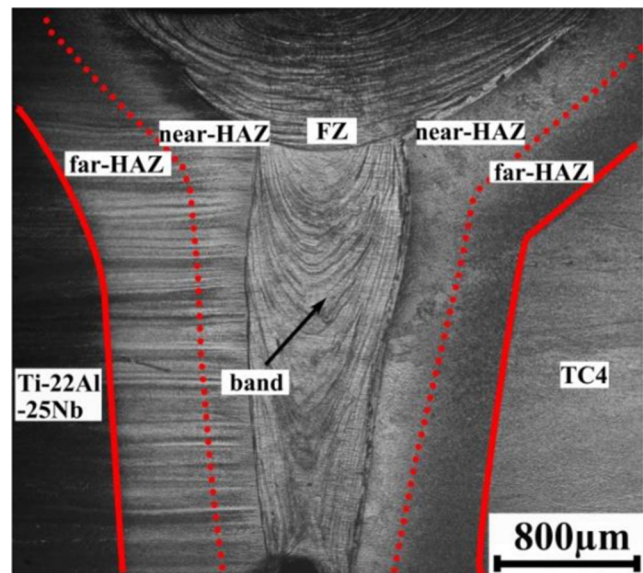

Fig. 2 Weld profiles of Ti-22Al-25Nb/TC4 dissimilar joint

molten zone ratios of Ti-22Al-25Nb and TC4 alloys are about 1/3 (82 blocks) and 2/3 (173 blocks) respectively. But when the electron beam aims at the assembly center, as shown in Fig. 4 b, the molten zone ratios of Ti-22Al-25Nb and TC4 alloys occupy about 3/7 (120 blocks) and 4/7 (156 blocks) respectively.

3.2 Microstructure characterization of welded joint

The microstructure of Ti-22Al-25Nb alloy consists of α_2, B2, and O phases [7, 10, 18, 19], as shown in Fig. 5 a, and the nominal chemical names of α_2, B2, and O are Ti_3Al, the ordered β, and Ti_2AlNb respectively. TC4 alloy is composed of bright α phase and dark β phase, as shown in Fig. 5 b.
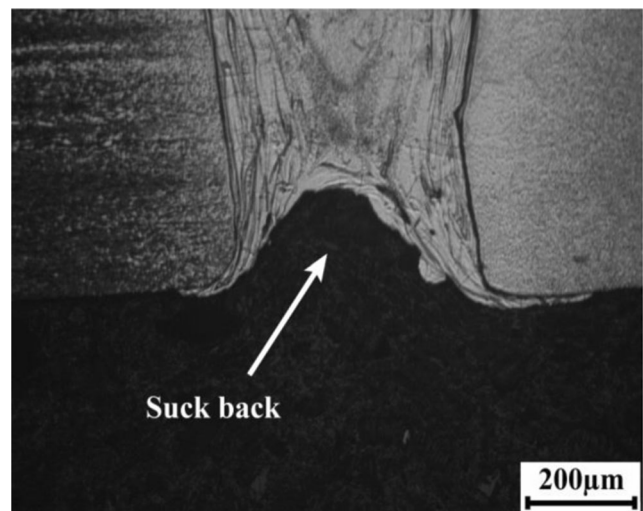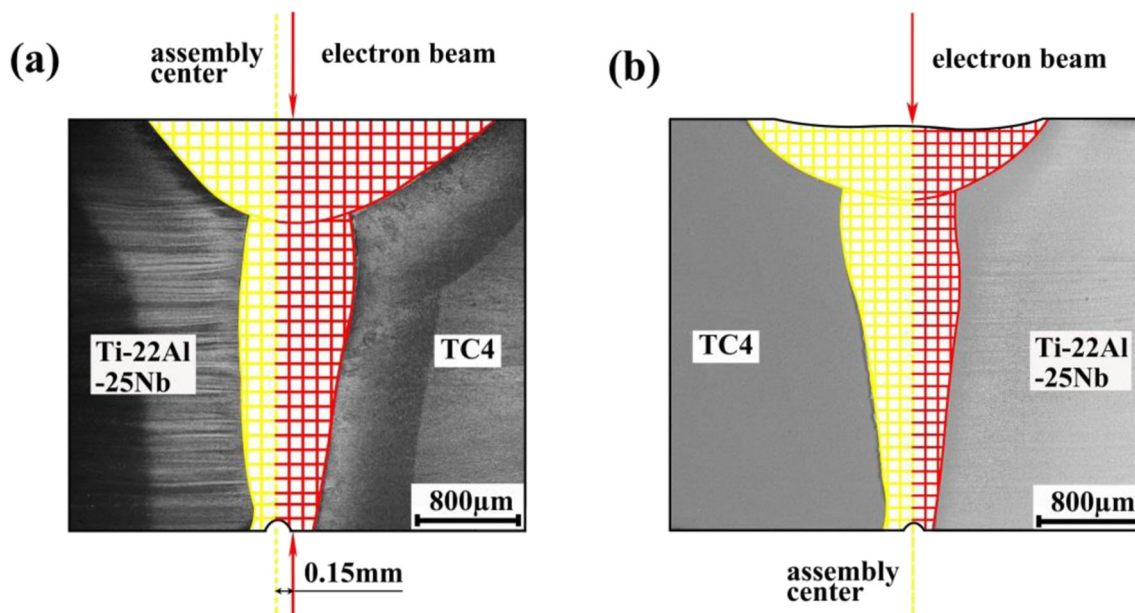

Fig. 3 Welding defect in joint #6

Fig. 4 Molten zone of base metal on both sides with computational grids. **a** Beam deviation to TC4 side. **b** Without beam deviation

Figure 6 shows the joint #2 microstructure in the HAZ of Ti-22Al-25Nb side. In the far-HAZ, there are O phase, B2 phase, and α_2 phases, but the quantity of O phase is lower than that in Ti-22Al-25Nb base metal (BM). With the distance away from FZ, the quantity of α_2 phase is decreased. There are B2 phase and a little of α_2 phase in the near-HAZ. According to the phase diagram of Ti-Al-Nb alloy [20], as to the alloy with chemical composition of 22Al (at%), its peak temperature was higher than the transition temperature of β/B2 phase, and it successively crossed through the $\alpha_2 +$ B2 + O, $\alpha_2 +$ B2, and B2 phase regions with the elevation of temperature. Shao et al. [21] investigated the phase transformation in Ti-22Al-25Nb alloy. Due to the high heating rate in EBW, the transformation from α_2 phase to B2 phase is probably insufficient in the near-HAZ. With the distance away from FZ, the peak temperature is gradually decreased. In the far-HAZ, the maximum temperature is lower than the

transition temperature of β/B2 phase, and the phase transition from O phase to α_2 phase and B2 phase will occur.

Figure 6 b shows that grains in the HAZ of the modification welding zone are coarser than that in the HAZ of the first bead welding zone, while the quantity of α_2 phase in the HAZ of the modification welding zone is less than that in the HAZ of the first bead welding zone. Heat input mainly focuses on the joint surface during the modification welding, and the upper part of joint is remelted. There are enough energy and longer time for both the grain growth and phase transformation from α_2 phase to B2/β phase.

The joint #2 microstructure is distinctly different in the HAZ of TC4 side. In the near-HAZ, martensitic α' phase with different sizes from 30 μm to 75 μm is distributed randomly, as shown in Fig. 7 a and b. There also exists basket-weave structure in the near-HAZ of TC4 side. The temperature in the near-HAZ is higher than the transition temperature of β phase
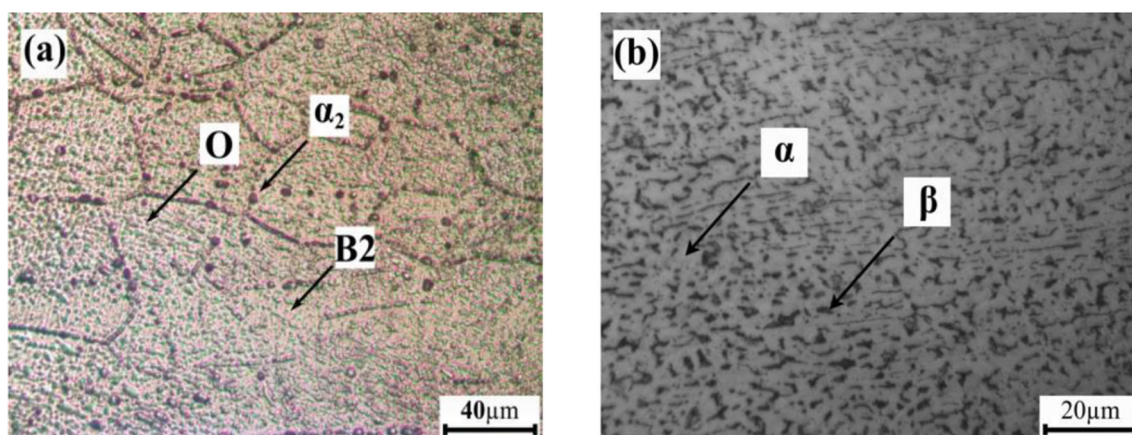

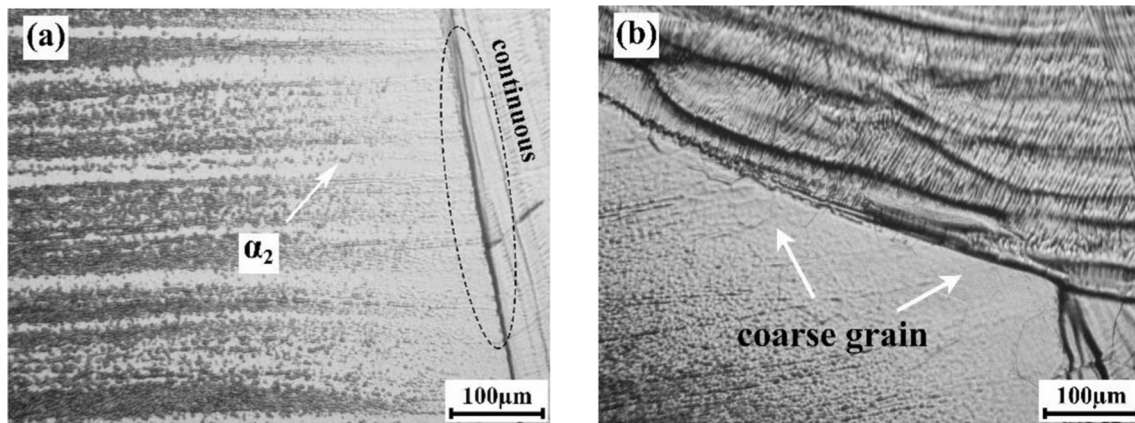**Fig. 5** Microstructure of base metals. **a** Ti-22Al-25Nb alloy. **b** TC4 alloy

Fig. 6 Joint #2 microstructure of HAZ in Ti-22Al-25Nb side. **a** The first bead welding zone. **b** The modification welding zone

in the heating process. Under the subsequent rapid cooling, β phase transforms into martensitic α′ phase. It was in accordance with the investigation on the welding of TC4 alloy [22–24]. With the distance away from fusion line, the size and quantity of martensitic α′ phase are decreased. In the near-HAZ of the modification welding zone, the martensitic α′ phase is coarser than that of in the first bead welding zone, as shown in Fig. 7 c. During the modification welding, the upper part of weldment is remelted, and there is enough

thermal energy to promote the growth of martensitic α′ phase in the near-HAZ. In the far-HAZ of TC4 side, there are primary α, transformed β, and acicular α phases, as shown in Fig. 7 a and d. Both the peak temperature and cooling rate in the far-HAZ are lower than that of in the near-HAZ, thus the microstructure in the far-HAZ is basically the same to that of the original TC4 alloy.

The microstructure of FZ is mainly composed of B2 phase and martensitic α′ phase. Columnar grains are perpendicular
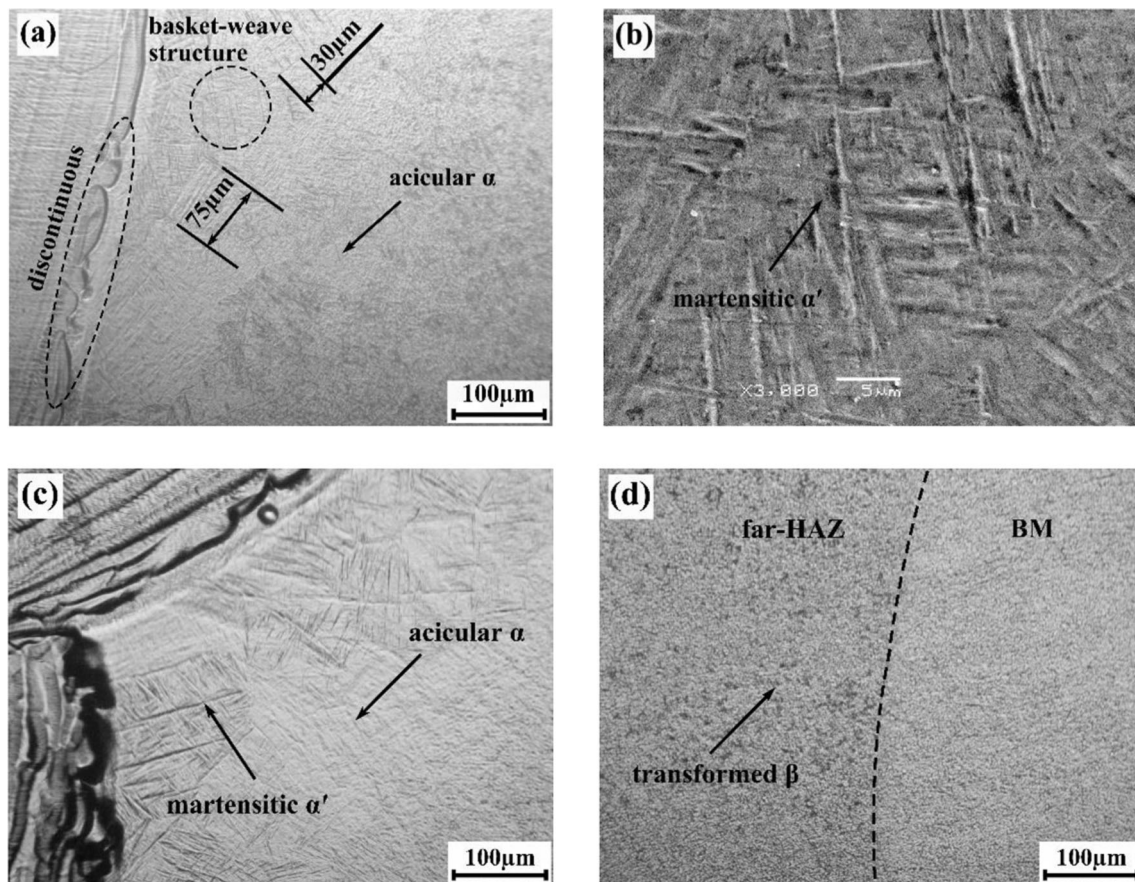

Fig. 7 Joint #2 microstructure of HAZ in TC4 side. **a** The first bead welding zone. **b** High magnification image of the first bead welding zone. **c** The modification welding zone. **d** Far-HAZ
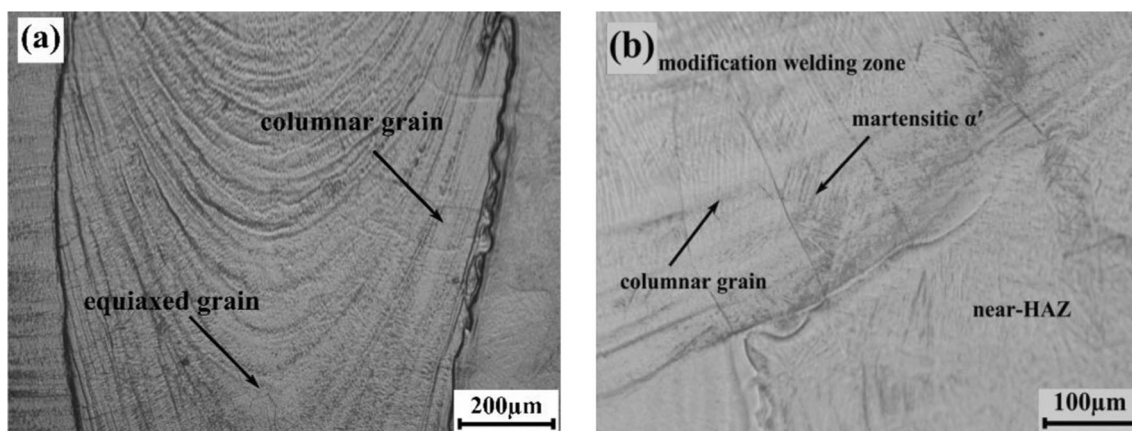
Fig. 8 Microstructure of FZ. **a** Low magnification of the first bead welding zone. **b** The modification welding zone

to fusion line and lamellar lines, as shown in Fig. 8 a. The segregation of alloying elements may contribute to forming lamellar lines by the electron beam oscillation during EBW process. The equiaxed grains are generated in the weld center. Figure 8 b shows the microstructure of FZ in the modification welding zone. The columnar grains are also perpendicular to fusion line, and grains grow up towards the weld center. The acicular-like phase distributes in the columnar grains zone. With the distance away from the weld center, the heat input is gradually decreased, thus the growth of columnar grains is in this way. As shown in Fig. 8 b, columnar grains in the modification welding zone are adjacent to the near-HAZ of TC4 side. Moreover, electron beam oscillation makes uniform distribution of alloying elements, and its chemical composition is almost unchanged in the FZ. Consequently, it can be inferred that the acicular phase is also martensitic α′ phase.

XRD pattern of the joint #2 weldment is shown in Fig. 9. It is further confirmed that the weldment consists of B2 phase and α′ phase. The peak intensity of B2 phase is very high, which indicates that there is mainly B2 phase in FZ. Microstructural evolution of welded joints depends on many factors, such as the original chemical composition and microstructure of base metals, and heating and cooling process during welding, etc. Generally, the following parameters were considered, such as heating rate, maximum temperature, cooling rate, and dwelling time at the evaluated temperature [24]. The maximum temperature is higher in the weld center, and the temperature gradient is larger near fusion line in both welding heating and cooling process. During welding, the cooling rate was higher than 120 K/s, which was the critical transition rate of β/B2 phase to O phase or α_2 phase [16, 25]. In the cooling stage, the β phase would transform into the ordered B2 phase. Consequently, there is mainly B2 phase in the FZ, and no O phase or α_2 phase is generated.

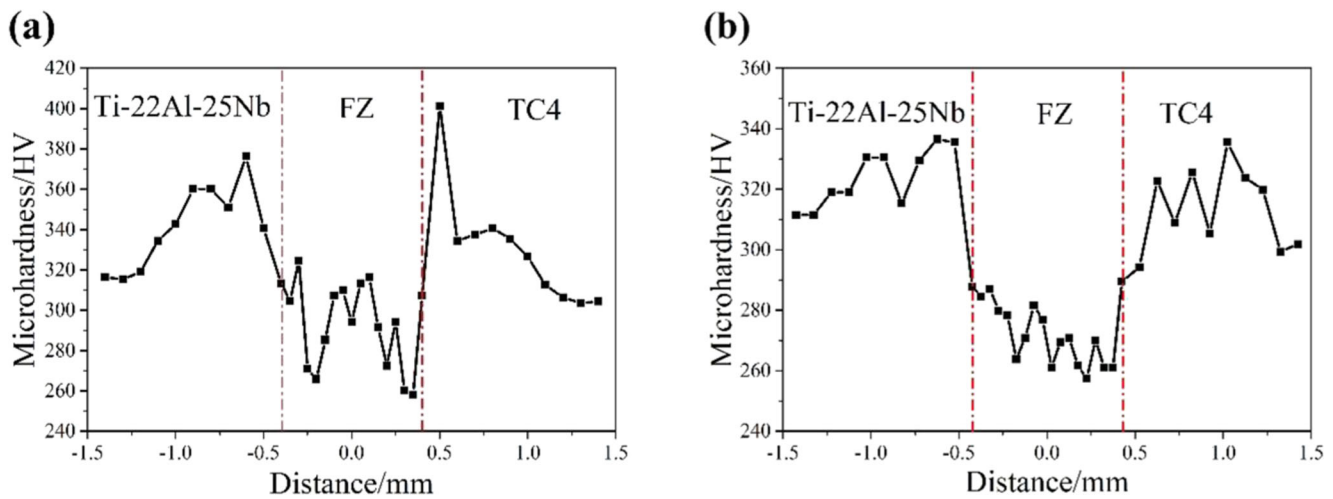**Fig. 9** XRD pattern of the weldment
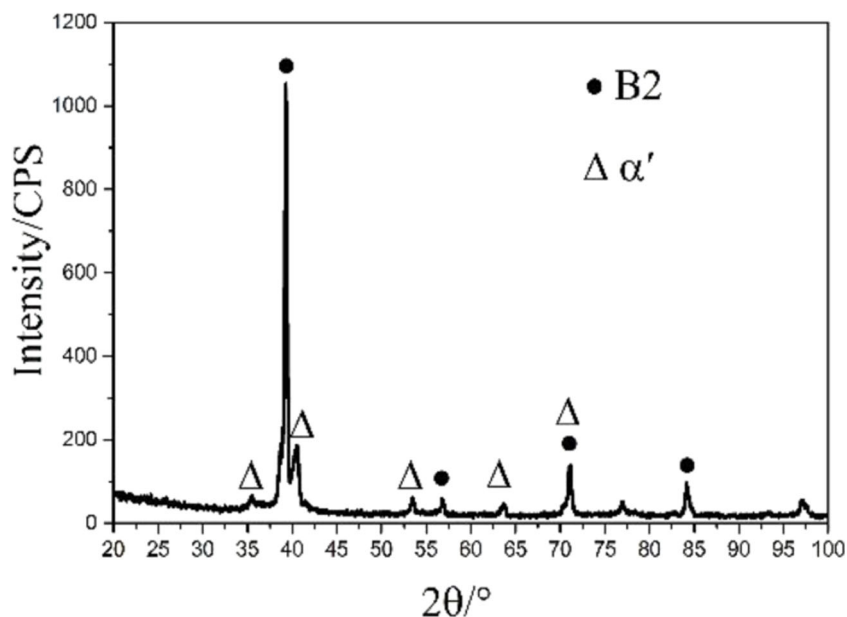
Fig. 10 Microhardness distribution of welded joints. **a** Without electron beam deviation. **b** With electron beam deviation

3.3 Mechanical properties and fracture analysis

After welding, the measurement samples of hardness are extracted from the middle part of welded joint, which are perpendicular to the weld center. The distribution curves of microhardness along the cross sections of joint #2 and joint #3 are depicted in Fig. 10. The microhardness distributions of two joints present M-type. Microhardness distribution of weld zone without electron beam deviation is roughly consistent with that with electron beam deviation to TC4 side. As shown in Fig. 10 a, without electron beam deviation during welding, the highest hardnesses in the HAZ of Ti-22Al-25Nb and TC4 sides are 376.2 HV and 401.3 HV respectively. However, with electron beam deviation during welding, the highest hardnesses in the HAZ of Ti-22Al-25Nb and TC4 sides are 336.5 HV and 335.5 HV respectively, as shown in Fig. 10 b. The hardness of weld zone is gradually decreased with the distance away from fusion line, and the lowest hardness appears in the weld center. The variation range of hardness value is 140 HV without beam deviation, while that is 80 HV with beam deviation. Obviously, the fluctuation of microhardness without beam deviation is larger than that of with beam deviation. Under the action of external stress, it

easily leads to stress concentration by the non-uniform distribution of microhardness.

The FZ consists of soft B2 phase and hard α' phase. According to the XRD analysis above, as shown in Fig. 9, the quantity of B2 phase is higher in the FZ. Therefore, the hardness of FZ mainly depends on the soft B2 phase. In the HAZ of TC4 side, the hardness of existing phases was ranked as follows: α' phase > α phase > β phase [22]. The near-HAZ mainly consists of martensitic α' phase, and base metal TC4 alloy is composed of α phase and β phase. Consequently, the hardness of near-HAZ is higher than that of base metal TC4 alloy. In the side of Ti-22Al-25Nb alloy, the hardness of HAZ is a little higher than that of base metal Ti-22Al-25Nb alloy. As shown in Figs. 6 and 7, the microstructure of far-HAZ is similar to that of base metal. Consequently, the hardness in these two regions is basically the same.

Perpendicular to the weld center, three parallel tensile samples are extracted from the middle part and two sides of the welded joint respectively. The results of tensile tests for the welded joints and base metals at room temperature are given in Table 2. It is the average of three measurements. The tensile strength of Ti-22Al-25Nb alloy approaches that of TC4 alloy, while its elongation is much lower than that of TC4 alloy,

Table 2 Results of tensile tests of base metals and dissimilar joints

Sample no.	Ultimate tensile strength (MPa)	Elongation (%)	Failure position
Ti-22Al-25Nb	1040.0	5.5	–
TC4	991.4	16.2	–
#1	917.9	1.9	FZ
#2	967.6	3.1	FZ
#3	945.9	1.6	FZ
#4	864.7	1.3	FZ
#5	893.5	1.4	FZ
#6	522.5	0.5	FZ

Fig. 11 Tensile fracture morphologies of welded joints. **a** Joint #1. **b** Joint #2
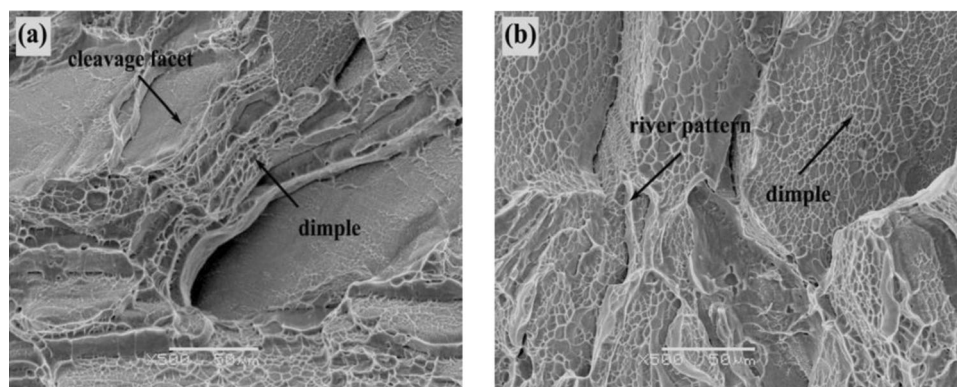
because the Ti-22Al-25Nb alloy is a kind of intermetallic compound, and its mechanical property is between that of the metal and ceramic [26]. Except for joint #6, the tensile strength of welded joints varied from 864.7 to 967.6 MPa, which reaches 83 to 93% of that of Ti-22Al-25Nb alloy, while the elongation of welded joints is 1.3 to 3.1%, which is greatly decreased compared with that of Ti-22Al-25Nb alloy. Because the FZ is composed of a lot of columnar grains, it is difficult to deform during stretching. As described in reference [23], the presence of martensitic α' phase could increase the tensile strength of welded joint but deteriorate its ductility. As for the welded joint #6, due to suck back, as shown in Fig. 3, both the tensile strength and elongation of joint #6 are the lowest. All the failure positions of welded joints locate in the FZ. It means that weld metal is the weak area in the welded joint.

Obviously, electron beam deviation contributes to both the tensile strength and elongation of dissimilar joint. When the electron beam is deviated to TC4 side, the more thermal energy can be supplied to it, thus the molten area of TC4 base metal occupies about 2/3 of FZ compared with that about 4/7 of FZ without beam deviation, as shown in Fig. 4. Because the TC4 alloy has good plasticity and toughness, the relatively large molten area in TC4 side may improve the elongation of welded joint to a certain extent. From Table 1, it can be seen that the appropriate heat input with or without beam deviation is 65.25 J/mm or 58.50 J/mm respectively. Compared with that without beam deviation, more thermal energy is needed to form good joints with beam deviation. It is relatively difficult for electron beam to penetrate weldment completely with beam deviation during welding.

Tensile fracture morphologies of joints #1 and #2 are shown in Fig. 11. Both of the two joints present the mixed mode of ductile and quasi-cleavage fracture. As shown in Fig. 11 a, there exist some dimples on the fracture surface of joint #1, and the cleavage facets appear simultaneously. Compared with that of joint #1, a little river pattern combined with a lot of equiaxed dimples distributes on the fracture surface of joint #2,

as shown in Fig. 11 b. The ductile characteristic of fracture surface is more obvious in the joint #2. It is consistent with the results of tensile tests in Table 2. The plasticity of dissimilar joint can be improved when the electron beam is deviated to TC4 side during welding.

3.4 Alloying elements distribution of weld zone

Alloying elements distribution of the joint #2 interface is shown in Figs. 12 and 13. It can be seen that, from Ti-22Al-25Nb side to TC4 side, the contents of elements Ti and V increase, while the content of element Nb decreases. The low content of element Al in weldment was advantageous to reducing the lattice aberrance and improving the ductility of joint [13]. The Al content in TC4 alloy is lower than that of in Ti-22Al-25Nb alloy. During welding, if the electron beam is deviated to TC4 side, the molten area of Ti-22Al-25Nb side can be reduced to a certain extent, as shown in Fig. 4 a, which results in the decrease of Al content in the FZ. Elements Nb and Ti distribute uniformly in the FZ, but the content of element Nb in TC4 side and the element Ti in Ti-22Al-25Nb side are decreased near fusion line, respectively. No obvious
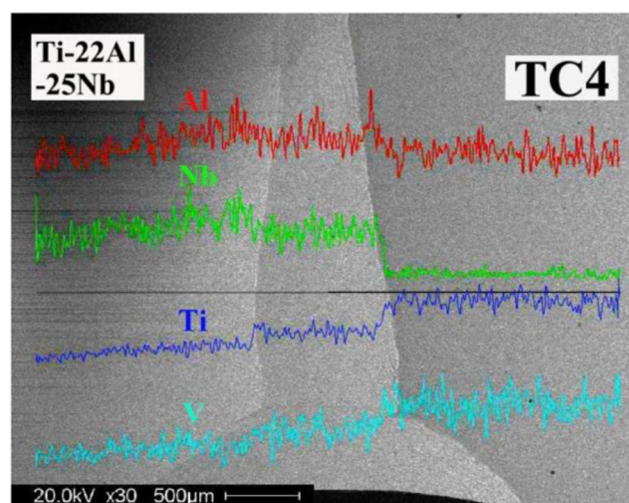

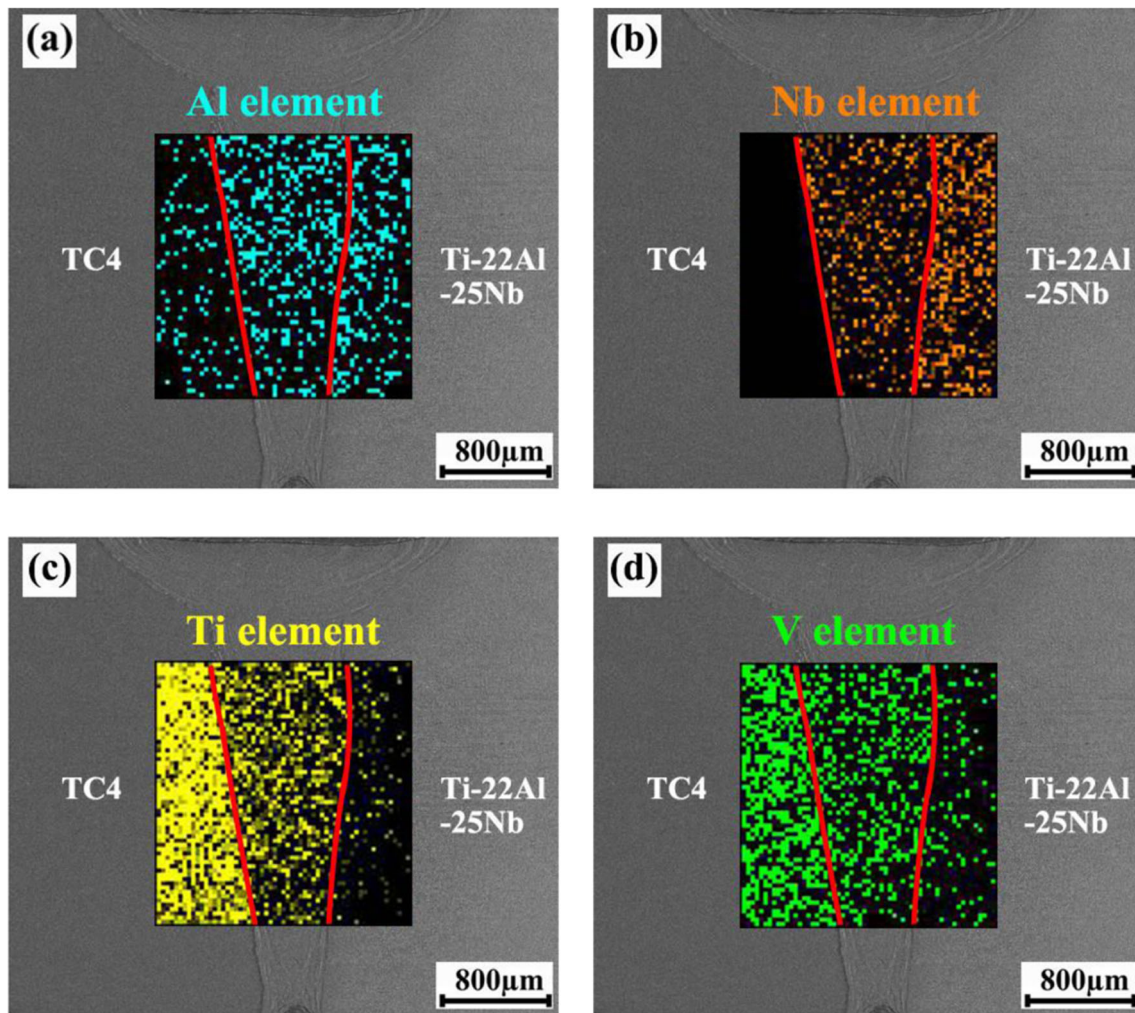**Fig. 12** Alloying elements distribution of weld zone

Fig. 13 Distribution of alloying elements in welded joint. **a** Al element. **b** Nb element. **c** Ti element. **d** V element

segregation of alloying elements appears in the weld zone. Consequently, it can be inferred that the molten pool is stirred fully during welding. There is a distinct boundary between the HAZ and FZ, as shown in Fig. 12. Due to the short dwelling time at high temperature and the rapid cooling rate in FZ, it has not enough time for the full diffusion of alloying elements during welding.

4 Conclusions

In present work, the Ti-22Al-25Nb/TC4 dissimilar alloys are welded with or without electron beam deviation respectively. The microstructure and mechanical properties of dissimilar joints are systematically investigated under different welding procedures. Some conclusions can be drawn as follows.

(1) The dissimilar joint consists of B2 phase and α' phase because of the rapid cooling rate during welding, which is higher than the critical cooling rate. In the HAZ of Ti-22Al-25Nb side, microstructure in near-HAZ is composed of B2 phase and a little of α_2 phase, while far-HAZ is made up of B2 phase, α_2 phase, and a little of O phase. In the HAZ of TC4 side, the near-HAZ is made up of martensitic α' phase, and the far-HAZ is composed of primary α, transformed β, and acicular α phases.

(2) Compared with that without electron beam deviation, more heat input is needed to form good dissimilar joint when electron beam is deviated to TC4 side with the distance of 0.15 mm during welding. Beam deviation can increase the tensile strength of welded joint to a certain extent and obviously improve the elongation of welded joint. Microhardness distribution of the welded joint is basically the same with or without beam deviation, but the variation range of hardness value in weld zone is 140 HV without beam deviation and 80 HV with beam deviation respectively.

(3) Electron beam oscillation can stir the molten pool fully, the main alloying elements distribute uniformly in the FZ, and no obvious segregation appears. Due to the rapid

cooling rate in EBW process, the diffusion of alloying elements is restrained to a certain extent. The content of element Nb in TC4 side and the element Ti in Ti-22Al-25Nb side are decreased near fusion line, respectively.

References

1. Tan LJ, Yao ZK, Wang T, Guo HZ (2011) Effect of post-weld heat treatment on microstructure and properties of electron beam welded joint of Ti$_2$AlNb/TC11. Mater Sci Technol 27(8):1315–1320
2. Skvortsova SV, Il'in AA, Mamonov AM, Nochovnaya NA, Umarova OZ (2016) Structure and properties of semifinished sheet products made of an intermetallic refractory alloy based on Ti$_2$AlNb. Mater Sci 51(6):821–826
3. Beddoes JC, Wallace W, de Malherbe MC (1992) The technology of titanium aluminides for aerospace applications. Mater Manuf Process 7(4):527–559
4. Zhang XS, Chen YJ, Hu JL (2018) Recent advances in the development of aerospace materials. Prog Aerosp Sci 97:22–34
5. Wang Y, Jiao M, Yang ZW, Liu YC (2018) Vacuum brazing of Ti$_2$AlNb and TC4 alloys using Ti-Zr-Cu-Ni and Ti-Zr-Cu-Ni+Mo filler metals: microstructural evolution and mechanical properties. Arch Civ Mech Eng 18(2):546–556
6. Casalino G, Mortello M (2016) Modeling and experimental analysis of fiber laser offset welding of Al-Ti butt joints. Int J Adv Manuf Technol 83(1–4):89–98
7. Zhang KZ, Ni LC, Lei ZL, Chen YB, Hu X (2016) Microstructure and tensile properties of laser welded dissimilar Ti-22Al-27Nb and TA15 joints. Int J Adv Manuf Technol 87(5–8):1685–1692
8. Shen JQ, Li B, Hu SS, Zhang H, Bu XZ (2017) Comparison of single-beam and dual-beam laser welding of Ti-22Al-25Nb/TA15 dissimilar titanium alloys. Opt Laser Technol 93:118–126
9. Li JJ, Shen JQ, Hu SS, Zhang H, Bu XZ (2019) Microstructure and mechanical properties of Ti-22Al-25Nb/TA15 dissimilar joint fabricated by dual-beam laser welding. Opt Laser Technol 109:123–130
10. Lei ZL, Dong ZJ, Chen YB, Huang L, Zhu RC (2013) Microstructure and mechanical properties of laser welded Ti-22Al-27Nb/TC4 dissimilar alloys. Mater Sci Eng A 559:909–916
11. Tan LJ, Yao ZK, Ning YQ, Guo HZ (2011) Effect of isothermal deformation on microstructure and properties of electron beam welded joint of Ti$_2$AlNb/TC11. Mater Sci Technol 27(9):1469–1474
12. Qin C, Yao ZK, Zhang DY, Ning YQ, Guo HZ, Zhao ZL (2013) Effect of hot work on stress rupture properties of electron beam welds of Ti-24Al-15Nb-1.5Mo/TC11 dual-alloy. Rare Metal Mater Eng 42(11):2207–2211
13. Chen GQ, Zhang BG, Liu W, Feng JC (2013) Influence of aluminum content on the microstructure and properties of electron beam welded joints of TiAl/TC4 alloy. Rare Metal Mater Eng 42(3):452–456
14. Fu PF, Mao ZY, Wang YJ, Tang ZY, Zuo CJ (2015) Fatigue properties of heavy-thickness Ti6.5Al2Zr1Mo1V alloy with oscillation EBW. Vacuum 121:230–235
15. Wang YJ, Fu PF, Guan YJ, Lu ZJ, Wei YT (2013) Research on modeling of heat source for electron beam welding fusion-solidification zone. Chin J Aeronaut 26(1):217–223
16. Chen YB, Zhang KZ, Hu X, Lei ZL, Ni LC (2016) Study on laser welding of a Ti-22Al-25Nb alloy: microstructural evolution and high temperature brittle behavior. J Alloys Compd 681:175–185
17. Liu QL, Li XM, Jiang YH (2017) Numerical simulation of EBCHM for the large-scale TC4 alloy slab ingot during the solidification process. Vacuum 141:1–9
18. Lei ZL, Dong ZJ, Chen YB, Zhang J, Zhu RC (2013) Microstructure and tensile properties of laser beam welded Ti-22Al-27Nb alloys. Mater Des 46:151–156
19. Li DL, Hu SS, Shen JQ, Zhang H, Bu XZ (2016) Microstructure and mechanical properties of laser-welded joints of Ti-22Al-25Nb/TA15 dissimilar titanium alloys. J Mater Eng Perform 25(5):1880–1888
20. Boehlert CJ, Majumdar BS, Seetharaman V, Miracle DB (1999) Part I. the microstructural evolution in Ti-Al-Nb O+BCC orthorhombic alloys. Metall Mater Trans A 30(9):2305–2323
21. Shao B, Zong YY, Wen DS, Tian YT, Shan DB (2016) Investigation of the phase transformations in Ti-22Al-25Nb alloy. Mater Charact 114:75–78
22. Lu W, Shi YW, Lei YP, Li XY (2012) Effect of electron beam welding on the microstructures and mechanical properties of thick TC4-DT alloy. Mater Des 34:509–515
23. Kumar C, Das M, Paul CP, Bindra KS (2018) Comparison of bead shape, microstructure and mechanical properties of fiber laser beam welding of 2 mm thick plates of Ti-6Al-4V alloy. Opt Laser Technol 105:306–321
24. Ma XY, Gong SL, Zhang JX, Lu W, Yang J (2016) Formation, microstructure and mechanical properties of double-sided laser beam welded Ti-6Al-4V T-joint. Trans Nonferrous Metals Soc China 26(3):729–735
25. Chen W, Li JW, Chen ZY, Wu CC, Tang ZY, Wang QJ (2016) Microstructure evolution and tensile properties of Ti-22Al-25Nb electron beam weld. Proceedings of the 13th World Conference on Titanium. John Wiley and Sons, Inc. 1243-1247
26. Zhang QC, Chen MH, Wang H, Wang N, Ouyang JD, Li XX (2016) Thermal deformation behavior and mechanism of intermetallic alloy Ti$_2$AlNb. Trans Nonferrous Metals Soc China 26(3):722–728